

BAYESIAN INFERENCE OF SOLAR AND STELLAR MAGNETIC FIELDS IN THE WEAK-FIELD APPROXIMATION

A. ASENSIO RAMOS

Instituto de Astrofísica de Canarias, 38205, La Laguna, Tenerife, Spain
 Departamento de Astrofísica, Universidad de La Laguna, E-38205 La Laguna, Tenerife, Spain
Draft version January 12, 2013

ABSTRACT

The weak-field approximation is one of the simplest models that allows us to relate the observed polarization induced by the Zeeman effect with the magnetic field vector present on the plasma of interest. It is usually applied for diagnosing magnetic fields in the solar and stellar atmospheres. A fully Bayesian approach to the inference of magnetic properties in unresolved structures is presented. The analytical expression for the marginal posterior distribution is obtained, from which we can obtain statistically relevant information about the model parameters. The role of a-priori information is discussed and a hierarchical procedure is presented that gives robust results that are almost insensitive to the precise election of the prior. The strength of the formalism is demonstrated through an application to IMaX data. Bayesian methods can optimally exploit data from filter-polarimeters given the scarcity of spectral information as compared with spectro-polarimeters. The effect of noise and how it degrades our ability to extract information from the Stokes profiles is analyzed in detail.

Subject headings: methods: data analysis, statistical — techniques: polarimetric — Sun: photosphere

1. INTRODUCTION

Extracting information about the magnetic field vector from spectro-polarimetric observations is not devoid of difficulties. The main one is that, practically always, one has to go through a modeling phase. This modeling typically consists of setting an atmospheric model that depends on some parameters which one wants to infer. Such a procedure, usually known as spectro-polarimetric inversion, has allowed to extract extremely valuable information about the behavior of the magnetic field in the solar photosphere and chromosphere (see e.g., Bellot Rubio 2006, and references therein).

It is hard to summarize in a few lines the history of spectro-polarimetric inversions from the first steps back in the 1970s. The initially proposed models were of low complexity because the quality of the observations and the computing power did not allow the use of more elaborate models (e.g., Auer et al. 1977; Skumanich & Lites 1987; Lites & Skumanich 1990; Keller et al. 1990). Although the assumptions on which these models are based may not be exactly fulfilled in the solar atmosphere, their simplicity allowed to put the cornerstone for quantitative spectropolarimetry. In fact, these models are still in use for interpreting high-quality observations from the most advanced instruments (Lagg et al. 2004; Orozco Suárez et al. 2007; Borrero et al. 2010). Later on, inversion codes based on the concept of response functions (Landi Degl’Innocenti & Landi Degl’Innocenti 1977) have facilitated the inversion of high-quality Stokes profiles making it possible to infer vertical stratifications of the magnetic properties of the atmosphere (Ruiz Cobo & del Toro Iniesta 1992; Socas-Navarro et al. 2000; Frutiger et al. 2000).

After the enormous success of standard inversion methods based on least-squares optimization, it is time to study in depth the inversion process itself and introduce more powerful techniques. This is what has been done recently by Asensio Ramos et al. (2007), who treated the inversion process as a Bayesian probabilistic inference problem. These techniques, which allow to fully exploit the information encoded in the Stokes profiles once a model has been proposed to explain them, have been used recently by Asensio Ramos (2009, 2010) to infer that fields in the quietest regions of the solar internetwork appear to be quasi-isotropically distributed, reinforcing the previous results of Martínez González et al. (2008). We consider that the Bayesian approach is the best choice, specially in those cases in which the spectro-polarimetric signal is at the noise level or the wavelength covering is very sparse (like in filter-polarimeters). Additionally, it gives the opportunity to quantitatively compare different models and use different models as a committee to gain insight on a common physical parameter (Asensio Ramos 2010).

The approach followed by Asensio Ramos et al. (2007) based on a Markov Chain Montecarlo sampler is completely general so that it can cope with very complex radiative transfer forward problems. The main drawback is that it can become costly in terms of computational time, although not prohibitive, as already shown by Asensio Ramos (2009). Obviously, Bayesian inference cannot be compared to standard inversion methods just by the computing cost, because the amount of information obtained is much richer. In order to motivate the application of Bayesian inference, we consider in this paper the assumption of weak field (Landi Degl’Innocenti & Landolfi 2004) for the inference of magnetic fields from the observation of Stokes profiles. This is one of the most straightforward approximations one can consider to relate the Stokes profiles and the magnetic field vector. In spite of its simplicity, its range of applicability is very broad and it is systematically applied in different fields, from solar to stellar physics, as shown in the next section. As we show, the simplicity of the model allows us to obtain analytical expression for some of the posterior distributions of the model parameters. We consider that the weak-field approximation is of practical application while simultaneously

being simple enough to demonstrate the power of Bayesian inference and show their fundamental points.

Section 2 describes the model. Section 3 shows the simple non-hierarchical approach and also sets the notation used throughout the paper. Section 4 presents the robust hierarchical model for the case in which the noise standard deviation is known and when it is inferred from the data. Finally, the method is demonstrated with some examples in section 5.

2. THE ZEEMAN WEAK-FIELD APPROXIMATION

When the splitting produced in a given spectral line via the Zeeman effect by the presence of a deterministic magnetic field ($\bar{g}\Delta\lambda_B$, with \bar{g} the effective Landé factor) is smaller than the line broadening ($\Delta\lambda_D$), the line is said to be well modeled in the weak-field regime (Landi Degl’Innocenti & Landi Degl’Innocenti 1973). Writing the expressions for $\Delta\lambda_B$ and $\Delta\lambda_D$ (e.g., Landi Degl’Innocenti & Landolfi 2004), a line is in the weak-field approximation when the magnetic field strength fulfills:

$$B < \frac{4\pi mc}{\bar{g}\lambda_0 e_0} \sqrt{\frac{2kT}{M} + v_{\text{mic}}}, \quad (1)$$

where m and e_0 are the electron mass and charge, respectively, c is the speed of light, k is the Boltzmann constant, M is the mass of the species, λ_0 is the central wavelength of the spectral line under consideration and v_{mic} is the microturbulent velocity. For an iron line at $\lambda_0 = 5000$ Å, using $v_{\text{mic}} = 1$ km s⁻¹ and $T = 5800$ K, we end up with:

$$\bar{g}B < 2400\text{G}. \quad (2)$$

In principle, this is more than enough to deal with photospheric magnetic fields outside from active regions in the solar atmosphere observed with magnetically sensitive lines in the optical (with $\bar{g} > 1$) or even active regions observed in lines with a weak magnetic sensitivity. Since the thermal width is enhanced in the chromosphere due to the increased temperature and the field strength is known to be smaller, the weak-field approximation is especially interesting for inferring magnetic fields at chromospheric heights.

In this approximation, a straightforward relation between the magnetic properties of the plasma and the emergent Stokes parameters exist. In present day observations of the weakly magnetized regions of the solar atmosphere we cannot state that we are resolving all magnetic structures. In case that our resolution element is not filled with an unidirectional magnetic field vector, we can mimic the loss of signal by assuming that the observed signal in the pixel is obtained as the average of a magnetic component with a relative weight f and a non-magnetic component with the weight $1 - f$. The following equations hold for Stokes V at first order in the field strength and for Stokes Q , U at second order in the field strength (e.g., Landi Degl’Innocenti & Landolfi 2004):

$$\begin{aligned} V(\lambda) &= \alpha f B_{\parallel} \frac{\partial I(\lambda)}{\partial \lambda} \\ Q(\lambda) &= \beta f B_{\perp}^2 \cos 2\chi \frac{\partial^2 I(\lambda)}{\partial \lambda^2} \\ U(\lambda) &= \beta f B_{\perp}^2 \sin 2\chi \frac{\partial^2 I(\lambda)}{\partial \lambda^2}, \end{aligned} \quad (3)$$

as functions of B_{\parallel} , the projection of the magnetic field vector along the line-of-sight (LOS), B_{\perp} , the component of the vector perpendicular to the LOS, χ , the field azimuth and $I(\lambda)$, the wavelength variation of the intensity across the spectral line. The proportionality constants α and β have the values:

$$\alpha = -4.67 \times 10^{-13} \bar{g} \lambda^2, \quad \beta = -5.45 \times 10^{-26} \bar{G} \lambda^4, \quad (4)$$

with the wavelength λ in Å and the components of the magnetic field measured in G. The factor \bar{g} is the effective Landé factor and \bar{G} is the equivalent for linear polarization (e.g., Landi Degl’Innocenti & Landolfi 2004). Both factors measure the sensitivity of the spectral line to the presence of a magnetic field. The previous expressions are only valid when B_{\parallel} , B_{\perp} , the field azimuth χ , the line-of-sight velocity, the Doppler width, and any broadening mechanism are constant with height in the line formation region. Additionally, the expression for Stokes Q and U can only be applied for non-saturated lines. Since the field azimuth is constant with height in the atmosphere, it is possible to define the total linear polarization $L = (Q^2 + U^2)^{1/2}$ which can be written as:

$$L = f B_{\perp}^2 \left| \beta \frac{\partial^2 I(\lambda)}{\partial \lambda^2} \right|, \quad (5)$$

where the absolute value is a consequence of the definition of L . From this point, we assume that $Q(\lambda)$, $U(\lambda)$ and $V(\lambda)$, the observed wavelength variation of the linear and circular polarization profiles, respectively, can be correctly modeled with the aid of Eqs. (3).

In spite of and thanks to its simplicity, the weak-field approximation is broadly applied for the inference of solar and stellar magnetic fields from the observation of Stokes profiles. A limited selection includes the detection and diagnostic of magnetic fields in: central stars of planetary nebulae (Jordan et al. 2005), white dwarfs (Aznar Cuadrado et al. 2004) pulsating stars (Silvester et al. 2009), hot subdwarfs (O’Toole et al. 2005), Ap and Bp stars (Wade et al. 2000) and

chemically peculiar stars (Bagnulo et al. 2002). The least-squares deconvolution (LSD) technique that is widely used for the detection of magnetic fields in solar-type stars (Donati et al. 1997) is also fundamentally based on the weak-field approximation. Many synoptic magnetographs like those of Big Bear (Sprock et al. 2001; Varsik 1995) are calibrated using this formalism or equivalent. The circular polarization observed in chromospheric lines like the 10830 Å multiplet of He I is very well modeled under the weak-field approximation (Merenda et al. 2006; Asensio Ramos et al. 2008). It is even used to produce modern vector magnetograms like those obtained with the IMAx instrument (Martínez Pillet et al. 2011) onboard the Sunrise balloon (Solanki et al. 2010).

3. NON-HIERARCHICAL BAYESIAN APPROACH

The weak-field approximation is a model for the interpretation of observed Stokes profiles that depends on the four-vector of parameters $(f, B_{\parallel}, B_{\perp}, \chi)$. Under the Bayesian approach (see Asensio Ramos et al. 2007; Asensio Ramos 2009, and references therein), all knowledge gained about the parameters when some dataset D is presented to the model is encoded on the posterior probability distribution function $p(f, B_{\parallel}, B_{\perp}, \chi|D)$. Using the Bayes theorem, this posterior distribution can be written as:

$$p(f, B_{\parallel}, B_{\perp}, \chi|D) = \frac{p(D|f, B_{\parallel}, B_{\perp}, \chi)p(f, B_{\parallel}, B_{\perp}, \chi)}{p(D)}, \quad (6)$$

where $p(D|f, B_{\parallel}, B_{\perp}, \chi)$ is the likelihood distribution that takes into account the influence of data on our knowledge of the model parameters and $p(f, B_{\parallel}, B_{\perp}, \chi)$ is the prior distribution that accounts for all information about the parameters known in advance. The term $p(D)$ is the evidence or marginal posterior (the area below the multidimensional posterior) that, for parameter inference, is just an unimportant multiplicative constant that we neglect in the following. We analyze now the analytical form of all quantities present in Eq. (6).

3.1. Likelihood

When Stokes profiles are observed with a spectro-polarimeter or a filter-polarimeter we measure the circular and linear polarization at N discrete wavelength points. Consequently, the observables are $\{(V_i, Q_i, U_i), i = 1, \dots, N\}$, where V_i , Q_i and U_i represent the value of the circular and linear polarization at wavelength λ_i , respectively. Assuming that the observations are corrupted with uncorrelated Gaussian noise with zero mean and variance σ_n^2 , the likelihood function is given by the following expression:

$$p(D|f, B_{\parallel}, B_{\perp}, \chi) = (2\pi)^{-3N/2} \sigma_n^{-3N} \exp \left\{ -\frac{1}{2\sigma_n^2} \left[\sum_{i=1}^N \left(V_i - \alpha f B_{\parallel} \frac{\partial I_i}{\partial \lambda} \right)^2 + \sum_{i=1}^N \left(Q_i - \beta f B_{\perp}^2 \cos 2\chi \frac{\partial^2 I_i}{\partial \lambda^2} \right)^2 + \sum_{i=1}^N \left(U_i - \beta f B_{\perp}^2 \sin 2\chi \frac{\partial^2 I_i}{\partial \lambda^2} \right)^2 \right] \right\} \quad (7)$$

where we have assumed that the total likelihood is given by the product of the likelihood for each wavelength point and Stokes parameter. Note that we have assumed the same noise variance for Stokes Q , U and V . If this is not the case, the likelihood can be modified accordingly and the following calculations are modified accordingly. Note also that we have assumed that the uncertainty in the first and second intensity derivatives are negligible. If this is not the case, its effect can be introduced by substituting σ_n^2 by the variance of the terms inside the parenthesis, which might also include correlations between (V_i, Q_i, U_i) and $\frac{\partial I_i}{\partial \lambda}$ or $\frac{\partial^2 I_i}{\partial \lambda^2}$. It is important to point out that the likelihood is only a Gaussian distribution if we deal with the observables $Q(\lambda)$ and $U(\lambda)$, and not for $L(\lambda)$. In this case, it would follow a Rayleigh distribution. Due to the simplicity of the weak-field model, the exponent of the likelihood can be easily factorized so that quantities related to observables are isolated from the model parameters. After some algebra, we end up with:

$$p(D|f, B_{\parallel}, B_{\perp}, \chi) = (2\pi)^{-3N/2} \sigma_n^{-3N} \exp \left[-(A_1 + A_2 f^2 B_{\parallel}^2 + A_3 f^2 B_{\perp}^4 - 2A_4 f B_{\parallel} - 2(A_5 \cos 2\chi + A_6 \sin 2\chi) f B_{\perp}^2) \right], \quad (8)$$

where the quantities A_i are the only ones that depend on the observations and are given by:

$$\begin{aligned} A_1 &= (2\sigma_n^2)^{-1} \sum_i (V_i^2 + Q_i^2 + U_i^2), & A_2 &= (2\sigma_n^2)^{-1} \alpha^2 \sum_i \left(\frac{\partial I_i}{\partial \lambda} \right)^2, & A_3 &= (2\sigma_n^2)^{-1} \beta^2 \sum_i \left(\frac{\partial^2 I_i}{\partial \lambda^2} \right)^2, \\ A_4 &= (2\sigma_n^2)^{-1} \alpha \sum_i V_i \frac{\partial I_i}{\partial \lambda}, & A_5 &= (2\sigma_n^2)^{-1} \beta \sum_i Q_i \frac{\partial^2 I_i}{\partial \lambda^2}, & A_6 &= (2\sigma_n^2)^{-1} \beta \sum_i U_i \frac{\partial^2 I_i}{\partial \lambda^2}. \end{aligned} \quad (9)$$

More intuition can be gained if we complete the squares in the likelihood function, so that:

$$p(D|f, B_{\parallel}, B_{\perp}, \chi) = (2\pi)^{-3N/2} \sigma_n^{-3N} \exp \left\{ -f^2 \left[A_2 \left(B_{\parallel} - \frac{A_4}{A_2 f} \right)^2 + A_3 \left(B_{\perp}^2 - \frac{A_5 \cos 2\chi + A_6 \sin 2\chi}{A_3 f} \right)^2 \right] \right\} \\ \times \exp \left\{ - \left[A_1 - \frac{A_4^2}{A_2} - \frac{(A_5 \cos 2\chi + A_6 \sin 2\chi)^2}{A_3} \right] \right\}, \quad (10)$$

3.2. Priors

One of the advantages of the Bayesian approach is that all a-priori information about model parameters is made explicit in the formalism. This is made through the probability distribution $p(f, B_{\parallel}, B_{\perp}, \chi)$. For simplicity, we assume that the prior distribution factorizes, so that:

$$p(f, B_{\parallel}, B_{\perp}, \chi) = p(f)p(B_{\parallel})p(B_{\perp})p(\chi). \quad (11)$$

Correlations between model parameters will then be obtained from the observed data through the likelihood. We do not have any preference for any specific value or the filling factor and the field azimuth, so we set uniform flat priors in the interval $[0, 1]$ and $[0, 2\pi]$, respectively. As a consequence, $p(f) = \Pi(f - 1/2)$ and $p(\chi) = (2\pi)^{-1} \Pi((2\pi)^{-1}(\chi - \pi))$, where $\Pi(x)$ is the standard rectangular function. If one wants to carry out the inference assuming $f = 1$, it is enough to set $p(f) = \delta(f - 1)$ and the following formulae are still valid. Concerning the components of the magnetic field, it is interesting to use priors that give low preference to very large values. We know that values above a few thousand G are not realistic. Instead of using a truncated flat prior, for computational purposes and inspired on physical considerations, we use different functional forms trying to be as non-informative as possible while maintaining physical constraints. For B_{\parallel} we propose a Gaussian distribution with a large variance σ_{\parallel}^2 , while for B_{\perp} we propose a Rayleigh distribution with large variance σ_{\perp}^2 , a consequence of the assumption of Gaussianity for the two components of the magnetic field perpendicular to the line-of-sight (LOS). If $\sigma_{\parallel} = \sigma_{\perp}$, we end up with an isotropic distribution for the magnetic field vector. The two parameters σ_{\parallel} and σ_{\perp} are known as hyperparameters because they parametrize the priors. The complete prior distribution is given by:

$$p(f, B_{\parallel}, B_{\perp}, \chi) = \Pi(f - 1/2) \frac{1}{2\pi} \Pi\left(\frac{\chi - \pi}{2\pi}\right) \left[\frac{1}{\sqrt{2\pi}\sigma_{\parallel}} \exp\left(-\frac{B_{\parallel}^2}{2\sigma_{\parallel}^2}\right) \right] \left[\sigma_{\perp}^{-2} B_{\perp} \exp\left(-\frac{B_{\perp}^2}{2\sigma_{\perp}^2}\right) \right]. \quad (12)$$

We note that any other functional form for the prior can be used if they are based on sensible physical intuition, although some of the following integrals may require more numerical work for their evaluation. As a rule, if data contains sufficient information about the model parameters, the results should be almost insensitive to the election of the prior as long as the prior gives non-negligible probability to the regions of high likelihood. For this reason, it is fundamental to compare the posterior with the chosen prior to know if data has added information to the inference problem. If they are very similar, the results depend on the specific election of the prior and should, in principle, be discarded.

3.3. Posterior

The full posterior distribution results from the application of Eq. (6):

$$p(f, B_{\parallel}, B_{\perp}, \chi|D) = \Pi(f - 1/2) \Pi\left(\frac{\chi - \pi}{2\pi}\right) (2\pi)^{-(3N+3)/2} \sigma_n^{-3N} \frac{1}{\sigma_{\parallel} \sigma_{\perp}^2} B_{\perp} \exp \left\{ - \left[A_1 + \left(A_2 f^2 + \frac{1}{2\sigma_{\parallel}^2} \right) B_{\parallel}^2 + \right. \right. \\ \left. \left. + A_3 f^2 B_{\perp}^4 - 2A_4 f B_{\parallel} - \left[2f(A_5 \cos 2\chi + A_6 \sin 2\chi) - \frac{1}{2\sigma_{\perp}^2} \right] B_{\perp}^2 \right] \right\}. \quad (13)$$

Since in the non-hierarchical model that we are dealing with in this section the normalizing constants are just a scale, they can be dropped without effect. They will be however important in the following section when marginalizing out the prior parameters. The following rewriting is also convenient for evaluating some of the marginal posterior for the components of the magnetic field vector:

$$p(f, B_{\parallel}, B_{\perp}, \chi|D) = \Pi(f - 1/2) \Pi\left(\frac{\chi - \pi}{2\pi}\right) (2\pi)^{-(3N+3)/2} \sigma_n^{-3N} \frac{1}{\sigma_{\parallel} \sigma_{\perp}^2} B_{\perp} \exp \left[-(B_1 - 2B_2 f + B_3 f^2) \right], \quad (14)$$

where

$$B_1 = A_1 + \frac{B_{\parallel}^2}{2\sigma_{\parallel}^2} + \frac{B_{\perp}^2}{2\sigma_{\perp}^2}, \quad B_2 = A_4 B_{\parallel} + (A_5 \cos 2\chi + A_6 \sin 2\chi) B_{\perp}^2, \quad B_3 = A_2 B_{\parallel}^2 + A_3 B_{\perp}^4. \quad (15)$$

The joint posterior distribution contains all information about the parameters of the weak-field approximation for a set of observed Stokes profiles. Different versions of the posterior can be built if different priors are assigned.

3.4. Maximum-a-posteriori and maximum-likelihood solutions

The maximum a-posteriori (MAP) solution to the problem (the one producing the largest posterior inside the prior volume) can be obtained by finding the value of $(f, B_{\parallel}, B_{\perp}, \chi)_{\text{MAP}}$ that maximizes Eq. (13), which is equivalent to minimizing $-\ln p(f, B_{\parallel}, B_{\perp}, \chi|D)$. The MAP solution is, therefore, the one minimizing:

$$\begin{aligned} -\ln p(f, B_{\parallel}, B_{\perp}, \chi|D) = & -\ln B_{\perp} + A_1 + \left(A_2 f^2 + \frac{1}{2\sigma_{\parallel}^2} \right) B_{\parallel}^2 + A_3 f^2 B_{\perp}^4 - 2A_4 f B_{\parallel} \\ & - \left[2f(A_5 \cos 2\chi + A_6 \sin 2\chi) - \frac{1}{2\sigma_{\perp}^2} \right] B_{\perp}^2 + \text{cte.} \end{aligned} \quad (16)$$

The solution can be found by solving the following non-linear system of equations:

$$\begin{aligned} -A_4 B_{\parallel} - A_5 B_{\perp}^2 + A_2 B_{\parallel}^2 f + A_3 B_{\perp}^4 f &= 0 \\ -A_4 f + B_{\parallel} \left(\frac{1}{2\sigma_{\parallel}^2} + A_2 f^2 \right) &= 0 \\ -\frac{1}{B_{\perp}} + 4A_3 B_{\perp}^3 f^2 - 2B_{\perp} \left[2(A_5 \cos 2\chi + A_6 \sin 2\chi) f - \frac{1}{2\sigma_{\perp}^2} \right] &= 0. \\ 4f B_{\perp}^2 A_5 \sin 2\chi - 4f B_{\perp}^2 A_6 \cos 2\chi &= 0. \end{aligned} \quad (17)$$

The last equation is the standard estimation of the field azimuth which, provided that $B_{\perp} \neq 0$ and $f \neq 0$, results in:

$$\tan 2\chi = \frac{A_6}{A_5}, \quad (18)$$

which can then be understood as the maximum-a-posteriori estimation of the field azimuth. Additionally, particularizing to the case of a longitudinal magnetograph (i.e., if we do not measure linear polarization), we find the obvious solution $f B_{\parallel} = A_4/A_2$, that has been already found by Martínez González & Bellot Rubio (2009). Note also that the standard maximum-likelihood solution (also known as least-squares solution) is obtained following the same scheme after setting $\sigma_{\parallel} \rightarrow \infty$ and $\sigma_{\perp} \rightarrow \infty$ and dropping the term $\ln B_{\perp}$ from Eq. (17).

3.5. Marginal posteriors

To fully take into account the presence of degeneracies among the model parameters in the Bayesian approach, we have to compute the marginal posterior distributions for every parameters individually. The marginal posterior is obtained by integrating out all parameters but the one of interest. For instance, the posterior for B_{\parallel} is computed as:

$$p(B_{\parallel}|D) = \int_0^{2\pi} d\chi \int_0^1 df \int_0^{\infty} dB_{\perp} p(f, B_{\parallel}, B_{\perp}, \chi|D). \quad (19)$$

This integration will introduce into the probability distribution of a given parameter all possible values of the rest of model parameters weighed by their associated probabilities. The advantage of the weak-field model is that some of these integrals can be obtained analytically in closed form. Due to the complexity of the integrals, we have been unable to find closed analytical expressions for the one-dimensional marginal distributions. However, we present in App. B the expressions for the 2-dimensional marginal posteriors $p(f, \chi|D)$ and for the 3-dimensional marginal posteriors $p(f, B_{\parallel}, B_{\perp}|D)$, $p(B_{\parallel}, B_{\perp}, \chi|D)$, $p(f, B_{\perp}, \chi|D)$ and $p(f, B_{\parallel}, \chi|D)$.

The shape of the marginal posterior is fundamental to decide whether a parameter is constrained or not by the observations. Although the solution to the problem would be to give the full marginal posteriors, it is sometimes interesting for presentation purposes to give a summary of the distribution. If there is a clear peak with tails falling to zero (like a Gaussian, but can often be asymmetric), the value of the parameter at the peak (the most probable) is the so-called marginal maximum-a-posteriori (MMAP) solution or mode. A confidence interval can be put by just integrating the posterior until a given fraction of the total area is obtained. Another possibility to summarize the distribution is to give the median value (where the cumulative probability distribution equals 1/2), together with a confidence region. Finally, it is possible to compute moments of the quantity x using the standard definition:

$$\langle x^n \rangle = \frac{\int x^n p(x|D) dx}{\int p(x|D) dx}, \quad (20)$$

and the confidence interval is obtained like in the MMAP.

3.6. Marginal posterior of derived quantities

Since all the information about the model parameters is contained in the posterior probability distribution function, information about any derived quantity can be computed from it using the machinery presented in App. A.

3.6.1. Magnetic flux density

One of the quantities of interest is the magnetic flux density, defined as $F_{\parallel} = fB_{\parallel}$. Following the change of variables formulae, we can write the probability distribution function of the magnetic flux density as:

$$\begin{aligned} p(F_{\parallel} \geq 0|D) &= \int_{F_{\parallel}}^{\infty} p\left(f = \frac{F_{\parallel}}{B_{\parallel}}, B_{\parallel} \middle| D\right) \frac{1}{|B_{\parallel}|} dB_{\parallel} \\ p(F_{\parallel} < 0|D) &= \int_{-\infty}^{-F_{\parallel}} p\left(f = \frac{F_{\parallel}}{B_{\parallel}}, B_{\parallel} \middle| D\right) \frac{1}{|B_{\parallel}|} dB_{\parallel} \end{aligned} \quad (21)$$

where the joint distribution $p(f, B_{\parallel}|D)$ is obtained by marginalizing B_{\perp} and χ from the full posterior. Since $0 \leq f \leq 1$, $|B_{\parallel}| \geq |F_{\parallel}|$ has to be fulfilled, which produces the separation of the integral in two different cases depending on the sign of F_{\parallel} . The integration on B_{\parallel} has to be carried out numerically since it is not possible to obtain a closed expression. The previous approach is unnecessarily complex for such a simple quantity like the magnetic flux density. In this special case, it can be computed following a different path, noting that the posterior for F_{\parallel} can also be obtained directly because:

$$V(\lambda) = \alpha F_{\parallel} \frac{\partial I(\lambda)}{\partial \lambda}, \quad (22)$$

and neither $Q(\lambda)$ nor $U(\lambda)$ do depend on F_{\parallel} . In such a case, it is easy to write a posterior for this variable:

$$p(F_{\parallel}|D) = p(F_{\parallel})(2\pi)^{-N/2} \sigma_n^{-N} \exp \left\{ -\frac{1}{2\sigma_n^2} \left[\sum_i V_i^2 + F_{\parallel}^2 \sum_i \alpha^2 \left(\frac{\partial I_i}{\partial \lambda} \right)^2 - 2F_{\parallel} \sum_i \alpha V_i \frac{\partial I_i}{\partial \lambda} \right] \right\}. \quad (23)$$

The only remaining ingredient is the prior distribution $p(F_{\parallel})$. Since $F_{\parallel} = fB_{\parallel}$ and the priors for f and B_{\parallel} have been discussed in Sec. 3.2, the prior for F_{\parallel} can be obtained following App. A, thus resulting in:

$$p(F_{\parallel}) = \frac{1}{2\sqrt{2\pi}\sigma_{\parallel}} E_1 \left(\frac{F_{\parallel}^2}{2\sigma_{\parallel}^2} \right), \quad (24)$$

where $E_1(x)$ is the first exponential integral (e.g., Abramowitz & Stegun 1972). When data is sufficiently informative so that the prior distribution becomes unimportant, the posterior for the magnetic flux density is Gaussian with mean and variance given by (Martínez González & Bellot Rubio 2009):

$$\begin{aligned} \mu(F_{\parallel}) &= \frac{\sum_i \alpha V_i \frac{\partial I_i}{\partial \lambda}}{\sum_i \alpha^2 \left(\frac{\partial I_i}{\partial \lambda} \right)^2} \\ \sigma^2(F_{\parallel}) &= \frac{\sigma^2}{\sum_i \alpha^2 \left(\frac{\partial I_i}{\partial \lambda} \right)^2}. \end{aligned} \quad (25)$$

3.6.2. Magnetic field inclination

A similar approach can be followed to compute the marginal posterior for the field inclination from the joint distribution of B_{\parallel} and B_{\perp} . To this end, we apply again the rules of App. A to the change of variables $\theta = \arctan(B_{\perp}/B_{\parallel})$ and obtain:

$$\begin{aligned} p(\theta \geq 0|D) &= |1 + \tan^2 \theta| \int_0^{\infty} dB_{\parallel} p(B_{\parallel}, B_{\perp} = B_{\parallel} \tan \theta | D) |B_{\parallel}| \\ p(\theta < 0|D) &= |1 + \tan^2 \theta| \int_{-\infty}^0 dB_{\parallel} p(B_{\parallel}, B_{\perp} = B_{\parallel} \tan \theta | D) |B_{\parallel}| \end{aligned} \quad (26)$$

where the joint distribution is computed by marginalizing f and χ from the posterior and the limits of integration have been adapted to fulfill $B_{\perp} = B_{\parallel} \tan(\theta) \geq 0$.

Using the same procedure, the prior distribution for the inclination can be obtained by plugging Eq. (12) into Eq. (26). The results is, after some algebra, that $p(\theta) = |\sin \theta|$, an obvious result because the prior we are using assumes that the field is isotropically distributed.

3.6.3. Magnetic field strength and energy

Exactly the same procedure can be applied to obtain the posterior for the magnetic field strength, $B = \sqrt{B_{\parallel}^2 + B_{\perp}^2}$, and to the magnetic field energy, $E_{\text{mag}} = B^2/8\pi$, obtaining:

$$\begin{aligned} p(B|D) &= \int_{-B}^B dB_{\parallel} \left| \frac{B}{\sqrt{B^2 - B_{\parallel}^2}} \right| p(B_{\parallel}, \sqrt{B^2 - B_{\parallel}^2} | D) \\ p(E_{\text{mag}}|D) &= \int_{-\sqrt{8\pi E_{\text{mag}}}}^{\sqrt{8\pi E_{\text{mag}}}} dB_{\parallel} \left| \frac{1}{\sqrt{8\pi E_{\text{mag}} - B_{\parallel}^2}} \right| p(B_{\parallel}, \sqrt{8\pi E_{\text{mag}} - B_{\parallel}^2} | D), \end{aligned} \quad (27)$$

where the joint probability distribution is computed by marginalizing f and χ from the posterior.

4. HIERARCHICAL BAYESIAN APPROACH

In principle, the values of σ_{\parallel} and σ_{\perp} in the previous formalism are understood to be fixed and given a-priori. One of the disadvantages of this approach is that, if there is not sufficient information about the model parameters encoded in the observations, the results will surely be sensitive to the election of these numbers (see §5 for an example). However, we can take advantage of the fact that, in the Bayesian formalism, every unknown can be considered a random variable. We can put an appropriate prior on them and extend the formalism in a hierarchical way and let data determine their values. Since the priors are put over hyperparameters (parameters of the prior distributions), they are known as hyperpriors. In principle, nothing avoids us to make hyperpriors depend on additional hyperparameters over which appropriate priors are assigned and continue the hierarchical structure (see, e.g., Gregory 2005; Gelman et al. 2003, for more details on hierarchical models). The immediate effect of the hierarchical approach is that results are much less dependent on the specific choice of hyperparameters and we make the problem essentially free of parameters. In some sense, this happens because we allow priors adapt to data. It can be demonstrated that some standard regularization schemes applied to least-squares techniques are indeed particular cases of hierarchical models.

4.1. Known noise variance

Using trivial probability calculus, the full posterior can be expressed by marginalizing out the hyperparameters, thus:

$$p(f, B_{\parallel}, B_{\perp}, \chi | D) = \int d\sigma_{\parallel} d\sigma_{\perp} p(D | f, B_{\parallel}, B_{\perp}, \chi) p(f, B_{\parallel}, B_{\perp}, \chi | \sigma_{\parallel}, \sigma_{\perp}) p(\sigma_{\parallel}, \sigma_{\perp}), \quad (28)$$

where we have used the fact that the likelihood does not depend on the parameters σ_{\parallel} and σ_{\perp} . Note that this marginalization takes into account *all* possible values of the hyperparameters weighted by their probability. The term $p(f, B_{\parallel}, B_{\perp} | \sigma_{\parallel}, \sigma_{\perp})$ is the prior defined in Eq. (12) and the new distribution $p(\sigma_{\parallel}, \sigma_{\perp})$ gives prior information about the hyperparameters. Since they behave as scale parameters (they can take values spanning several decades), a good option is to use a uniform prior on logarithmic scale, so that:

$$p(\sigma_{\parallel}, \sigma_{\perp}) = \frac{1}{\sigma_{\parallel}} \frac{1}{\sigma_{\perp}}. \quad (29)$$

This prior, also known as Jeffreys' prior (Jeffreys 1961; MacKay 2003), has the remarkable property of being the only non-informative prior for scale-invariant quantities. This complicates the analytical solution of the problem requiring more purely numerical integrations but also introduces additional stabilization. Although the Jeffreys' prior is improper (its integral is not finite), the integral of the priors over σ_{\parallel} and σ_{\perp} are finite but also improper. The integral of Eq. (28) can be finally carried out for all possible values of σ_{\parallel} and σ_{\perp} to give:

$$p(f, B_{\parallel}, B_{\perp}, \chi | D) = p(D | f, B_{\parallel}, B_{\perp}) \Pi(f - 1/2) \frac{1}{4\pi} \Pi\left(\frac{\chi - \pi}{2\pi}\right) \frac{1}{|B_{\parallel}| B_{\perp}}, \quad (30)$$

where the likelihood $p(D | f, B_{\parallel}, B_{\perp})$ is given by Eq. (8). The marginalization process demonstrates that the Jeffreys' prior is a natural election for B_{\parallel} and B_{\perp} . In other words, we could have started our calculation by selecting a Jeffreys' prior in Eq. (12) without considering the hierarchical approach.

In case no information is present in the data (flat likelihood), the prior for F_{\parallel} can be obtained by substitution of the previous expression in Eq. (21):

$$p(F_{\parallel}) = \frac{1}{|F_{\parallel}|}, \quad (31)$$

so the posterior is given by Eq. (23).

It is also possible to introduce new free hyperparameters σ_{\min} and σ_{\max} that define a lower and upper estimation of the width of the prior distributions, respectively. Although they constitute a new set of free parameters, the hierarchical character offers the advantage that results are much less sensitive to their exact values. Because we do not expect magnetic fields in the solar atmosphere larger than ~ 4000 G or we do not expect to detect fields below ~ 0.1

G, it is sensible to choose $\sigma_{\min} = 0.1$ G and $\sigma_{\max} = 4000$ G. These values can be adapted for specific cases (inverting Stokes profiles observed in active regions or the quiet Sun) but the results are really insensitive to the specific values, as shown in §5. The following prior is the resulting one after marginalizing out σ_{\parallel} and σ_{\perp} :

$$p(f, B_{\parallel}, B_{\perp}, \chi) = \Pi(f - 1/2) \frac{1}{4\pi} \Pi\left(\frac{\chi - \pi}{2\pi}\right) \frac{1}{B_{\parallel} B_{\perp}} \left[\operatorname{erf}\left(\frac{B_{\parallel}}{\sqrt{2}\sigma_{\min}}\right) - \operatorname{erf}\left(\frac{B_{\parallel}}{\sqrt{2}\sigma_{\max}}\right) \right] \\ \times \left[\exp\left(-\frac{B_{\perp}^2}{2\sigma_{\max}^2}\right) - \exp\left(-\frac{B_{\perp}^2}{2\sigma_{\min}^2}\right) \right], \quad (32)$$

which converges to Eq. (30) when $\sigma_{\min} = 0$ and $\sigma_{\max} \rightarrow \infty$. The function $\operatorname{erf}(x)$ is the error function (e.g., Abramowitz & Stegun 1972). This yields the following general expression for the posterior that we use when the noise variance is known:

$$p(f, B_{\parallel}, B_{\perp}, \chi | D) = \frac{1}{2} \Pi(f - 1/2) \Pi\left(\frac{\chi - \pi}{2\pi}\right) (2\pi)^{-(3N+1)/2} \sigma_n^{-3N} \\ \times \exp\left[-\left(A_1 + A_2 f^2 B_{\parallel}^2 + A_3 f^2 B_{\perp}^4 - 2A_4 f B_{\parallel} - 2(A_5 \cos 2\chi + A_6 \sin 2\chi) f B_{\perp}^2\right)\right] \\ \times \frac{1}{B_{\parallel} B_{\perp}} \left[\operatorname{erf}\left(\frac{B_{\parallel}}{\sqrt{2}\sigma_{\min}}\right) - \operatorname{erf}\left(\frac{B_{\parallel}}{\sqrt{2}\sigma_{\max}}\right) \right] \left[\exp\left(-\frac{B_{\perp}^2}{2\sigma_{\max}^2}\right) - \exp\left(-\frac{B_{\perp}^2}{2\sigma_{\min}^2}\right) \right]. \quad (33)$$

Again, we have been unable to obtain the 1-dimensional marginal distributions, but App. B presents the 3-dimensional marginal posteriors $p(f, B_{\parallel}, B_{\perp} | D)$ and $p(B_{\parallel}, B_{\perp}, \chi | D)$. In this generalized case, under non-informative data, the prior for F_{\parallel} results in:

$$p(F_{\parallel}) = \frac{1}{F_{\parallel}} \left[\operatorname{erf}\left(\frac{F_{\parallel}}{\sqrt{2}\sigma_{\min}}\right) - \operatorname{erf}\left(\frac{F_{\parallel}}{\sqrt{2}\sigma_{\max}}\right) \right] + \frac{1}{\sqrt{2\pi}\sigma_{\min}} E_1\left(\frac{F_{\parallel}^2}{2\sigma_{\min}^2}\right) - \frac{1}{\sqrt{2\pi}\sigma_{\max}} E_1\left(\frac{F_{\parallel}^2}{2\sigma_{\max}^2}\right) \quad (34)$$

which reduces to Eq. (31) when $\sigma_{\min} = 0$ and $\sigma_{\max} \rightarrow \infty$. Substitution in Eq. (23) gives the posterior for F_{\parallel} .

4.2. Unknown noise variance

Another step forward in the hierarchical model can be given if the noise standard deviation is not known with precision. Sometimes the peculiarities of the observation induce that estimating the observational uncertainty is not an easy task. It is typically estimated assuming ergodicity and calculating the variance of the signal on a continuum window, where the polarimetric signal is assumed to be zero. This might be flawed if, for instance, the polarimetric signal is very broad and the assumption of zero signal in the continuum window is not correct. Likewise, when there is a large velocity field producing a large Doppler shift, neighboring spectral lines can enter into the continuum window and give wrong estimation of the observational uncertainty. This is especially relevant when when observing with filter-polarimeters, where the information of the continuum is usually contained in one or two spectral samples. In such a case, it is possible to consider σ_n as a random variable which is marginalized at the end. Although we assume that the variance of the observational uncertainty is unknown, we postulate that the noise follows a Gaussian distribution. This distribution, in the absence of detailed information about the correct distribution apart from the finite variance, is the one suggested by the principle of maximum entropy. Therefore:

$$p(f, B_{\parallel}, B_{\perp}, \chi | D) = \int d\sigma_{\parallel} d\sigma_{\perp} d\sigma_n p(D | f, B_{\parallel}, B_{\perp}, \chi, \sigma_n) p(f, B_{\parallel}, B_{\perp}, \chi | \sigma_{\parallel}, \sigma_{\perp}) p(\sigma_{\parallel}, \sigma_{\perp}) p(\sigma_n). \quad (35)$$

Using a Jeffreys' prior over σ_n , so that $p(\sigma_n) = \sigma_n^{-1}$, integrating over the full domain in σ_n , σ_{\parallel} and σ_{\perp} , we obtain the following posterior:

$$p(f, B_{\parallel}, B_{\perp}, \chi | D) = \frac{1}{2} \Pi(f - 1/2) \Pi\left(\frac{\chi - \pi}{2\pi}\right) \frac{1}{|B_{\parallel}| |B_{\perp}|} (2\pi)^{-(3N+1)/2} C^{-3N/2}, \quad (36)$$

where

$$C = A'_1 + A'_2 f^2 B_{\parallel}^2 + A'_3 f^2 B_{\perp}^4 - 2A'_4 f B_{\parallel} - 2(A'_5 \cos 2\chi + A'_6 \sin 2\chi) f B_{\perp}^2, \quad (37)$$

the A'_i are obtained from the A_i defined in Eq. (9) but dropping the terms $(2\sigma_n^2)^{-1}$ and N is the number of wavelength points in the profiles. If we limit the integration to the range $[\sigma_{n_{\min}}, \sigma_{n_{\max}}]$ because we know that noise cannot be too small or too large, but keep the integration on the full space for σ_{\parallel} and σ_{\perp} we end up with the following posterior:

$$p(f, B_{\parallel}, B_{\perp}, \chi | D) = \frac{1}{2} \Pi(f - 1/2) \Pi\left(\frac{\chi - \pi}{2\pi}\right) \frac{1}{|B_{\parallel}| |B_{\perp}|} (2\pi)^{-(3N+1)/2} \\ \times C^{-3N/2} \left[\Gamma\left(\frac{3N}{2}, \frac{C}{2\sigma_{n_{\max}}^2}\right) - \Gamma\left(\frac{3N}{2}, \frac{C}{2\sigma_{n_{\min}}^2}\right) \right], \quad (38)$$

which reduces to Eq. (36) when $\sigma_{n_{\min}} \rightarrow 0$ and $\sigma_{n_{\max}} \rightarrow \infty$ due to the properties of the incomplete Gamma function $\Gamma(a, x)$ (e.g., Abramowitz & Stegun 1972). It is also possible to limit the integration volume in σ_n , σ_{\parallel} and σ_{\perp} , arriving at the most general hierarchical model we consider that can be applied when the noise variance is unknown:

$$p(f, B_{\parallel}, B_{\perp}, \chi|D) = \frac{1}{2} \Pi(f - 1/2) \Pi\left(\frac{\chi - \pi}{2\pi}\right) (2\pi)^{-(3N+1)/2} C^{-3N/2} \left[\Gamma\left(\frac{3N}{2}, \frac{C}{2\sigma_{n_{\max}}^2}\right) - \Gamma\left(\frac{3N}{2}, \frac{C}{2\sigma_{n_{\min}}^2}\right) \right] \\ \times \frac{1}{B_{\parallel} B_{\perp}} \left[\operatorname{erf}\left(\frac{B_{\parallel}}{\sqrt{2}\sigma_{\min}}\right) - \operatorname{erf}\left(\frac{B_{\parallel}}{\sqrt{2}\sigma_{\max}}\right) \right] \left[\exp\left(-\frac{B_{\perp}^2}{2\sigma_{\max}^2}\right) - \exp\left(-\frac{B_{\perp}^2}{2\sigma_{\min}^2}\right) \right]. \quad (39)$$

Concerning the posterior for the magnetic flux density, marginalizing Eq. (23) over σ_n with the Jeffreys' prior, we find:

$$p(F_{\parallel}|D) = p(F_{\parallel})(2\pi)^{-3N/2} D^{-N/2} \left[\Gamma\left(\frac{N}{2}, \frac{D}{2\sigma_{n_{\max}}^2}\right) - \Gamma\left(\frac{N}{2}, \frac{D}{2\sigma_{n_{\min}}^2}\right) \right], \quad (40)$$

where

$$D = \sum_i V_i^2 + F_{\parallel}^2 \sum_i \alpha^2 \left(\frac{\partial I_i}{\partial \lambda} \right)^2 - 2F_{\parallel} \sum_i \alpha V_i \frac{\partial I_i}{\partial \lambda}. \quad (41)$$

The prior distribution $p(F_{\parallel})$ can be that of Eq. (31) or the most general one of Eq. (34).

5. ILLUSTRATIVE EXAMPLES

5.1. Observed profile

In order to illustrate the behavior of the non-hierarchical and hierarchical models that we have developed, let us consider extracting information under the weak-field approximation from the wavelength variation of a selected Stokes profile observed with IMAx (Martínez Pillet et al. 2004; Martínez Pillet et al. 2011) onboard Sunrise (Solanki et al. 2010) in a quiet region of the solar atmosphere. The observed profile is shown in Fig. 1. The reason for choosing this instrument is to show the power of Bayesian methods to deal with cases in which there is reduced information in the observables. The number of sampled points is just 5 which makes the typical shape of the polarization profiles hardly indistinguishable. In order to apply the previous formulation we need to have an estimation of the first and second derivative of the Stokes I profile. The poor spectral sampling makes this operation delicate. However, we have decided to apply a numerical derivative based on a standard 3-point Lagrange interpolation of the profile. This could have been improved by, for instance, fitting the intensity profile to a Gaussian and using this fitted profile to carry out the derivative. We have verified that differences are negligible with both approaches.

Figure 2 shows the joint posterior marginal distributions $p(B_{\parallel}, B_{\perp}|D)$ in the first column, $p(f, B_{\parallel}|D)$ in the second one and $p(f, B_{\perp}|D)$ in the third. These marginal distributions help us distinguish which parameters are degenerate and help us understand the behavior of the full posterior. For comparison, the first two rows (labeled *a*) present cases obtained by marginalization of the non-hierarchical posterior of Eq. (13). Specifically, these panels were obtained by numerical integration of Eq. (B1). The middle two rows (labeled *b*) are obtained marginalizing the hierarchical posterior of Eq. (33) assuming Gaussian noise with a standard deviation of $\sigma_n = 2 \times 10^{-3}$ in units of the continuum intensity. Specifically, they are computed by numerical integration of Eq. (B7). Finally, the last two rows (labeled *c*) are obtained applying a numerical quadrature to the full hierarchical posterior of Eq. (39) that marginalizes the noise. Two typical values of the hyperparameters are considered in each one of the posteriors. The values of the relevant parameters are indicated in each plot and in the caption. As a general rule, the non-hierarchical model has a stronger sensitivity to the prior hyperparameters than the hierarchical models (e.g., Gelman et al. 2003). In our case, the hierarchical models are almost insensitive to the exact values of the hyperparameters, even though we have used two extreme values. The joint marginal posteriors clearly indicate the presence of strong degeneracies between the f and B_{\parallel} and B_{\perp} , as widely known. However, there is still some information available in the observations about each parameter individually, at least sufficient to discard regions of the space of parameters. Although part of this information is encoded in the priors, it is transparently introduced and can be controlled at will. Furthermore, this information is based on very general considerations about the behavior of the magnetic field (like typical maximum values present in the solar atmosphere).

When extracting information for a given parameter, it is necessary to marginalize out the rest of parameters. This marginalization carries out error propagation correctly and degeneracies are evidenced as long tails in the marginal posteriors. Figure 3 presents these posteriors. The first column corresponds to the non-hierarchical model, while the second and third columns are the results of the two hierarchical models. They were obtained numerically by integrating the distributions shown in Fig. 2. The first row is the marginal posterior for f , the second for B_{\parallel} , the third for B_{\perp} and the fourth for F_{\parallel} . The dashed lines are the priors considered for each parameter. In the non-hierarchical model, the MMAP value for B_{\parallel} seems to be relatively robust to the election of the prior, while it has a larger dependence on the prior for B_{\perp} and f . According to the shapes of the marginal posterior distributions, it is possible to give the most probable value together with asymmetric error bars which contain 68% or 95% of the total mass of the distribution. In this particular example, the lower limit of B_{\parallel} will be much larger in magnitude than the upper limit. The reason is that the sign of B_{\parallel} controls the sign of the Stokes V profile, and positive fields are strongly discarded by data

because the polarity is not the correct one. The same applies to f and B_{\perp} , which have a very asymmetric confidence interval. Interestingly, since F_{\parallel} is a quantity directly proportional to the amplitude of Stokes V in the weak-field regime, its marginal posterior distribution is very well determined and its width is fundamentally characterized by the noise standard deviation.

Given the sensitivity to the election of the prior of the non-hierarchical model, we also consider the two hierarchical models. The results are very robust to the election of the hyperparameters (the red and black curves overlap). The filling factor is not constrained at all by the observations, as expected in the weak-field regime. In spite of that, the posterior for the component of the field along the line-of-sight is constrained and one can define a MMAP value and a confidence interval. In any case, the analysis discards positive values and very large negative values of B_{\parallel} . Concerning B_{\perp} , the posterior is very similar to the prior. Since the prior is based on physical considerations, we can safely give an upper limit to B_{\perp} , but always taking into account that this comes essentially from a-priori knowledge.

The posterior for F_{\parallel} is again very close to a Gaussian with mean and variance given by Eq. (25) in the case of the hierarchical model with known noise. Note also that there is an additional peak at zero magnetic flux density. This peak is produced by the marginalization over the priors, which opens the possibility that the observed Stokes V signal is compatible with the absence of magnetic field. Concerning the hierarchical model with unknown noise standard deviation, the posterior is slightly narrower, induced by the Jeffreys' prior.

Finally, Fig. 4 presents the marginal posteriors for the derived quantities θ , B and E_{mag} , that were obtained numerically by integrating the distributions shown in Fig. 2 using the appropriate change of variables. The results indicate that we can put upper limits to the field strength and to the magnetic energy, and that data contains some information on these two variables, with posterior clearly different from the priors. Concerning the field inclination, the marginal posterior looks like the prior distribution, so that we can only discard positive inclinations because they are not compatible with the Stokes V profile polarity.

5.2. Degradation of information. The effect of noise

There are two important ingredients that differentiate a standard maximum-likelihood (or least-squares) approach and a Bayesian approach. The first one is that the solution to the inference problem is given in terms of marginal posterior distributions that already encode error propagation. The second is that, thanks to the effect of the priors, when noise is too large, the marginal posteriors resemble the prior. This way, one can clearly state when a parameter is constrained by data and avoid biased estimators. To show this effect, we have analyzed how the influence of noise modifies the marginal posteriors. We consider the Stokes profiles of the Fe I line at 6302.4904 Å synthesized using the Milne-Eddington approximation with $B = 400$ G, $\theta = 30^\circ$ and $\chi = 20^\circ$. This line has a large magnetic sensitivity, with $\bar{g} = 2.5$ and $G = 6.25$. Considering $f = 1$, the amplitude of Stokes V is of the order of 2% in units of the continuum intensity, I_c , while that of Stokes Q and V is of the order of 0.03% in the same units. We corrupt these profiles with Gaussian noise with zero mean and standard deviations $\sigma_n = \{5 \times 10^{-4}, 10^{-3}, 5 \times 10^{-3}, 10^{-2}\}$ in units I_c . The case with the smallest σ_n results in a noise amplitude of roughly the same amplitude of the linear polarization signal. We use the hierarchical model with known noise variance of Eq. (33) and numerically calculate the marginal posteriors. The results are shown in Fig. 5 for all physical parameters of relevance. Each color corresponds to a different value of σ_n . The vertical dotted lines indicate the maximum-likelihood values that maximize Eq. (8). The curves are slightly dependent on the actual noise realization because the A_i coefficients change. We plot the results for only one noise realization.

As a consequence of the selected values for the magnetic field vector and f , the original synthetic profile corresponds to $B_{\parallel} = 346.4$ G and $B_{\perp} = 200$ G. The marginal posterior for B_{\parallel} indicates that the MMAP value is compatible with the correct value only when the noise is not too large so that the Stokes V signal is not too perturbed. As soon as the noise increases, there is a shift towards smaller B_{\parallel} . An interesting property of the solution is that the confidence intervals are extremely asymmetric, with small values of B_{\parallel} absolutely discarded and a very large upper limit. This is produced, among other things, by the marginalization of the filling factor. Something similar happens for the field strength.

Concerning B_{\perp} , the marginal posterior is different from the prior only for $\sigma_n = 5 \times 10^{-4}$, with a bump roughly close to the correct value although displaced towards smaller values. As soon as the noise increases, there is no remaining information about this component of the field on the profiles and one can only put an upper limit. A consequence of this is the fact that the marginal posterior for the azimuth is essentially flat. Some peaks of larger probability are located close to the correct value but without statistical relevance. Since the field inclination depends on B_{\parallel} and B_{\perp} , the marginal posterior for the inclination indicates that a reliable inclination is only inferred when noise is sufficiently small. For large noises, only upper limits can be correctly defined. Finally, the marginal posteriors for the magnetic flux density are Gaussian with a variance proportional to the noise standard deviation (in G), as shown in Eq. (25).

6. CONCLUSIONS

We have considered the complete Bayesian inference of the parameters of a model based on the weak-field approximation to explain observed Stokes profiles¹. The simplicity of the approximation has allowed us to obtain a closed analytical expression for the posterior distribution function and for some of the ensuing marginal posteriors. Thanks to the Bayesian approach, prior information is transparently introduced into the problem. We have verified that results are sensitive to the hyperparameters of the prior and we have developed a hierarchical approach based on physical

¹ Computer programs that calculate all the quantities presented in this paper can be freely obtained from <http://www.iac.es/project/magnetism>.

arguments that introduce regularization into the problem. As a consequence, marginal posteriors are almost insensitive to the exact value of the hyperparameters. Using the Bayesian approach we are able to extract not only most probable values but also confidence intervals for the model parameters. This Bayesian approach can be of interest for filter-polarimetric data in which the line profiles are only sampled in a reduced number of wavelengths. Likewise, signals very close to the noise can be treated under this formalism avoiding biased estimations that plague least-squares solutions. It is left for the future to carry out a profound analysis of the biases introduced by least-squares solutions using the expressions introduced in this paper.

I thank R. Manso Sainz for fruitful discussions that led to improvements on the original manuscript. I also thank C. Beck and M. J. Martínez González for useful suggestions and V. Martínez Pillet for providing the IMaX data used in Section 5. Financial support by the Spanish Ministry of Science and Innovation through projects AYA2010-18029 (Solar Magnetism and Astrophysical Spectropolarimetry) is gratefully acknowledged.

APPENDIX

CHANGE OF VARIABLES

Given two random variables x and y with joint distribution $p(x, y)$, the probability distribution $q(w)$ for the derived quantity $w = f(x, y)$ with $f(x, y)$ invertible can be obtained following the standard chain of variables rule. If we define the auxiliar variable $z = g(x, y)$, we can write the following direct and inverse relations:

$$\begin{aligned} w &= f(x, y), & x &= \xi(z, w) \\ z &= g(x, y), & y &= \gamma(z, w). \end{aligned} \quad (\text{A1})$$

As a consequence, the joint probability distribution of z and w can be written as:

$$q(z, w) = p(\xi(z, w), \gamma(z, w)) |J|, \quad (\text{A2})$$

where J is the Jacobian of the transformation equation given by Eq. (A1):

$$J = \begin{vmatrix} \frac{\partial \xi(z, w)}{\partial z} & \frac{\partial \xi(z, w)}{\partial w} \\ \frac{\partial \gamma(z, w)}{\partial z} & \frac{\partial \gamma(z, w)}{\partial w} \end{vmatrix} = \begin{vmatrix} 1 & 0 \\ \frac{\partial \gamma(z, w)}{\partial z} & \frac{\partial \gamma(z, w)}{\partial w} \end{vmatrix} = \frac{\partial \gamma(z, w)}{\partial w}, \quad (\text{A3})$$

were the last two steps assumes $\xi(z, w) = z$ to simplify computations. The probability distribution $q(w)$ is obtained by marginalizing z from Eq. (A2):

$$q(w) = \int dz p(z, \gamma(z, w)) \left| \frac{\partial \gamma(z, w)}{\partial w} \right|. \quad (\text{A4})$$

For instance, if we want to carry out the transformation $w = f(x, y) = xy$, then $\gamma(z, w) = w/z$, so that

$$q(w) = \int dz p\left(z, \frac{w}{z}\right) \left| \frac{1}{z} \right|. \quad (\text{A5})$$

MARGINAL POSTERiors

This appendix presents some of the analytical posteriors that can be obtained from Eqs. (13) and (33).

Non-hierarchical model

If we integrate the field azimuth from the posterior of the non-hierarchical model, we obtain:

$$\begin{aligned} p(f, B_{\parallel}, B_{\perp} | D) &= \Pi(f - 1/2) \Pi\left(\frac{\chi - \pi}{2\pi}\right) (2\pi)^{-(3N+1)/2} \sigma_n^{-3N} \frac{1}{\sigma_{\parallel} \sigma_{\perp}^2} B_{\perp} I_0\left(2f B_{\perp}^2 \sqrt{A_5^2 + A_6^2}\right) \\ &\times \exp\left\{-\left[A_1 + \left(A_2 f^2 + \frac{1}{2\sigma_{\parallel}^2}\right) B_{\parallel}^2 + A_3 f^2 B_{\perp}^4 - 2A_4 f B_{\parallel} + \frac{B_{\perp}^2}{2\sigma_{\perp}^2}\right]\right\} \end{aligned} \quad (\text{B1})$$

where $I_0(x)$ is the modified Bessel function of the first kind (Abramowitz & Stegun 1972). It might be useful to apply the following series expansion of $I_0(x)$ to further integrate out the filling factor:

$$I_0(x) = \sum_{k=0}^{\infty} \left(\frac{1}{k!}\right)^2 \left(\frac{x}{2}\right)^{2k} = 1 + \frac{x^2}{4} + \frac{x^4}{64} + \dots \quad (\text{B2})$$

Likewise, marginalizing B_{\parallel} and B_{\perp} , we obtain:

$$\begin{aligned}
p(f, \chi|D) = & \frac{1}{8} \Pi(f - 1/2) \Pi\left(\frac{\chi - \pi}{2\pi}\right) (2\pi)^{-(3N+1)/2} \sigma_n^{-3N} \frac{1}{\sigma_{\parallel} \sigma_{\perp}^2} \frac{1}{f \left[A_3 \left((2\sigma_{\parallel}^2)^{-1} + A_2 f^2 \right) \right]^{1/2}} \\
& \times \exp \left[-A_1 + \frac{((2\sigma_{\perp}^2)^{-1} - 2(A_5 \cos 2\chi + A_6 \sin 2\chi)f)^2}{4A_3 f^2} + \frac{A_4^2 f^2}{(2\sigma_{\parallel}^2)^{-1} + A_2 f^2} \right] \\
& \times \left[1 + \operatorname{erf} \left(\frac{-(2\sigma_{\perp}^2)^{-1} + 2(A_5 \cos 2\chi + A_6 \sin 2\chi)f}{2\sqrt{A_3}f} \right) \right]. \tag{B3}
\end{aligned}$$

Concerning the marginal posterior for the field components, we have been unable to find a close analytical expression for the probability distributions $p(B_{\parallel}|D)$ and $p(B_{\perp}|D)$ because B_{\parallel} and B_{\perp} appear very intricately. However, the marginal posteriors can be obtained using adequate numerical quadrature methods on any of the following joint posteriors:

$$\begin{aligned}
p(B_{\parallel}, B_{\perp}, \chi|D) = & \frac{1}{2\sqrt{2}} \Pi\left(\frac{\chi - \pi}{2\pi}\right) (2\pi)^{-(3N+2)/2} \sigma_n^{-3N} \frac{1}{\sigma_{\parallel} \sigma_{\perp}^2} B_{\perp} (A_2 B_{\parallel}^2 + A_3 B_{\perp}^4)^{-1/2} \\
& \times \exp \left(-A_1 + \frac{B_{\parallel}^2}{2\sigma_{\parallel}^2} + \frac{B_{\perp}^2}{2\sigma_{\perp}^2} + \frac{(A_4 B_{\parallel} + (A_5 \cos 2\chi + A_6 \sin 2\chi) B_{\perp}^2)^2}{A_2 B_{\parallel}^2 + A_3 B_{\perp}^4} \right) \\
& \times \left[\operatorname{erf} \left(\frac{A_4 B_{\parallel} + (A_5 \cos 2\chi + A_6 \sin 2\chi) B_{\perp}^2}{\sqrt{A_2 B_{\parallel}^2 + A_3 B_{\perp}^4}} \right) \right. \\
& \left. - \operatorname{erf} \left(\frac{A_4 B_{\parallel} + (A_5 \cos 2\chi + A_6 \sin 2\chi) B_{\perp}^2 - A_2 B_{\parallel}^2 - A_3 B_{\perp}^4}{\sqrt{A_2 B_{\parallel}^2 + A_3 B_{\perp}^4}} \right) \right] \tag{B4}
\end{aligned}$$

$$\begin{aligned}
p(f, B_{\perp}, \chi|D) = & \frac{1}{\sqrt{2}} \Pi(f - 1/2) \Pi\left(\frac{\chi - \pi}{2\pi}\right) (2\pi)^{-(3N+2)/2} \sigma_n^{-3N} \frac{1}{\sigma_{\parallel} \sigma_{\perp}^2} \frac{B_{\perp}}{\sqrt{(2\sigma_{\parallel}^2)^{-1} + A_2 f^2}} \\
& \times \exp \left\{ \frac{A_4^2 f^2}{(2\sigma_{\parallel}^2)^{-1} + A_2 f^2} - A_1 + \left[2(A_5 \cos 2\chi + A_6 \sin 2\chi)f - \frac{1}{2\sigma_{\perp}^2} \right] B_{\perp}^2 - A_3 f^2 B_{\perp}^4 \right\} \tag{B5}
\end{aligned}$$

$$\begin{aligned}
p(f, B_{\parallel}, \chi|D) = & \frac{1}{4\sqrt{2}} \Pi(f - 1/2) \Pi\left(\frac{\chi - \pi}{2\pi}\right) (2\pi)^{-(3N+2)/2} \sigma_n^{-3N} \frac{1}{\sigma_{\parallel} \sigma_{\perp}^2} \frac{1}{\sqrt{A_3}f} \\
& \times \exp \left[\frac{(4\sigma_{\perp}^2)^{-2} - (A_5 \cos 2\chi + A_6 \sin 2\chi)(2\sigma_{\perp}^2)^{-1} - (A_1 A_3 + A_5^2 - \frac{A_3 B_{\perp}^2}{8\sigma_{\parallel}^2})f^2 + 2A_4 f^3 - A_2 B_{\parallel} f^4}{A_3 f^2} \right] \\
& \times \left[1 + \operatorname{erf} \left(\frac{-(2\sigma_{\perp}^2)^{-1} + 2(A_5 \cos 2\chi + A_6 \sin 2\chi)f}{2\sqrt{A_3}f} \right) \right]. \tag{B6}
\end{aligned}$$

The previous expressions can be particularized to the specific case of a longitudinal magnetograph, in which only circular polarization is observed. We obtain such a case making $A_3 = A_5 = A_6 = 0$, dropping Q_i and U_i from A_1 and making $\sigma_{\perp} \rightarrow \infty$.

Hierarchical model

Starting from Eq. (33), we have integrated out the field azimuth, yielding:

$$\begin{aligned}
p(f, B_{\parallel}, B_{\perp}|D) = & \frac{1}{2} (2\pi)^{-(3N-1)/2} \sigma_n^{-3N} \Pi(f - 1/2) \\
& \times \exp \left[- \left(A_1 + A_2 f^2 B_{\parallel}^2 + A_3 f^2 B_{\perp}^4 - 2A_4 f B_{\parallel} \right) \right] I_0 \left(2f B_{\perp}^2 \sqrt{A_5^2 + A_6^2} \right) \\
& \times \frac{1}{B_{\parallel} B_{\perp}} \left[\operatorname{erf} \left(\frac{B_{\parallel}}{\sqrt{2}\sigma_{\min}} \right) - \operatorname{erf} \left(\frac{B_{\parallel}}{\sqrt{2}\sigma_{\max}} \right) \right] \left[\exp \left(-\frac{B_{\perp}^2}{2\sigma_{\max}^2} \right) - \exp \left(-\frac{B_{\perp}^2}{2\sigma_{\min}^2} \right) \right] \tag{B7}
\end{aligned}$$

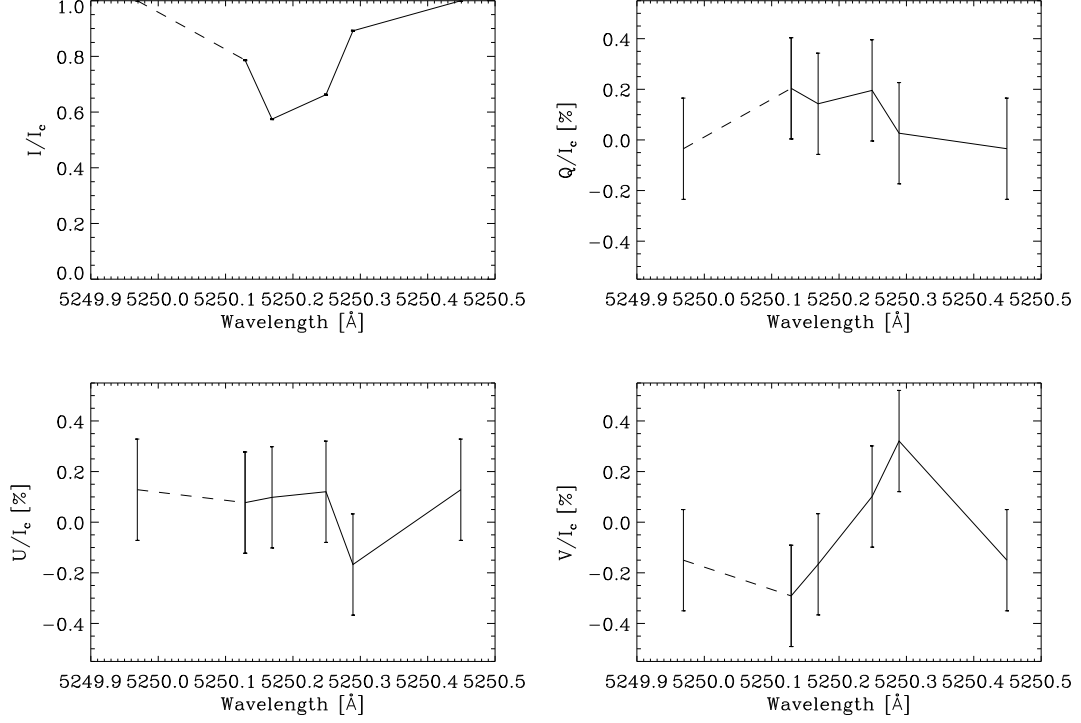


Figure 1. Stokes profiles observed with IMAx and used in the examples. The profiles consist of 5 wavelength points that have been obtained with a Fabry-Perot filter-polarimeter. For a better visualization, we have repeated the continuum point at 5250.45 Å symmetrically on the red wing, and connected it with dashed lines. We have also marked the uncertainty (estimated standard deviation of the noise) in each observed point with error bars.

Finally, it is possible to analytically integrate out f :

$$\begin{aligned}
 p(B_{\parallel}, B_{\perp}, \chi | D) &= \frac{1}{2} (2\pi)^{-3N/2} \sigma_n^{-3N} \Pi \left(\frac{\chi - \pi}{2\pi} \right) (A_2 B_{\parallel}^2 + A_3 B_{\perp}^4)^{-1/2} \\
 &\times \exp \left(-A_1 + \frac{(A_4 B_{\parallel} + (A_5 \cos 2\chi + A_6 \sin 2\chi) B_{\perp}^2)^2}{A_2 B_{\parallel}^2 + A_3 B_{\perp}^4} \right) \\
 &\times \left[\operatorname{erf} \left(\frac{A_4 B_{\parallel} + (A_5 \cos 2\chi + A_6 \sin 2\chi) B_{\perp}^2}{\sqrt{A_2 B_{\parallel}^2 + A_3 B_{\perp}^4}} \right) \right. \\
 &\quad \left. - \operatorname{erf} \left(\frac{A_4 B_{\parallel} + (A_5 \cos 2\chi + A_6 \sin 2\chi) B_{\perp}^2 - (A_2 B_{\parallel}^2 + A_3 B_{\perp}^4)}{\sqrt{A_2 B_{\parallel}^2 + A_3 B_{\perp}^4}} \right) \right] \\
 &\times \frac{1}{B_{\parallel} B_{\perp}} \left[\operatorname{erf} \left(\frac{B_{\parallel}}{\sqrt{2}\sigma_{\min}} \right) - \operatorname{erf} \left(\frac{B_{\parallel}}{\sqrt{2}\sigma_{\max}} \right) \right] \left[\exp \left(-\frac{B_{\perp}^2}{2\sigma_{\max}^2} \right) - \exp \left(-\frac{B_{\perp}^2}{2\sigma_{\min}^2} \right) \right]. \quad (\text{B8})
 \end{aligned}$$

REFERENCES

- Abramowitz, M., & Stegun, I. A. 1972, *Handbook of Mathematical Functions* (New York: Dover)
- Asensio Ramos, A. 2009, *ApJ*, 701, 1032
- Asensio Ramos, A. 2010, in *Solar Polarization 6*, ASP Conf. Ser.
- Asensio Ramos, A., Martínez González, M. J., & Rubiño Martín, J. A. 2007, *A&A*, 476, 959
- Asensio Ramos, A., Trujillo Bueno, J., & Landi Degl’Innocenti, E. 2008, *ApJ*, 683, 542
- Auer, L. H., House, L. L., & Heasley, J. N. 1977, *Sol. Phys.*, 55, 47
- Aznar Cuadrado, R., Jordan, S., Napiwotzki, R., Schmid, H. M., Solanki, S. K., & Mathys, G. 2004, *A&A*, 423, 1081
- Bagnulo, S., Szeifert, T., Wade, G. A., Landstreet, J. D., & Mathys, G. 2002, *A&A*, 389, 191
- Bellot Rubio, L. R. 2006, in *ASP Conf. Ser.*, Vol. 358, *Solar Polarization Workshop 4*, ed. R. Casini & B. W. Lites, 107
- Borrero, J. M., Tomczyk, S., Kubo, M., Socas-Navarro, H., Schou, J., Couvidat, S., & Bogart, R. 2010, *Sol. Phys.*, 35
- Donati, J.-F., Semel, M., Carter, B. D., Rees, D. E., & Collier Cameron, A. 1997, *MNRAS*, 291, 658
- Frutiger, C., Solanki, S. K., Fligge, M., & Bruls, J. H. M. J. 2000, *A&A*, 358, 1109
- Gelman, A., Carlin, J. B., Stern, H. S., & Rubin, D. B. 2003, *Bayesian Data Analysis*, Second Edition (Chapman & Hall/CRC Texts in Statistical Science) (Chapman & Hall)

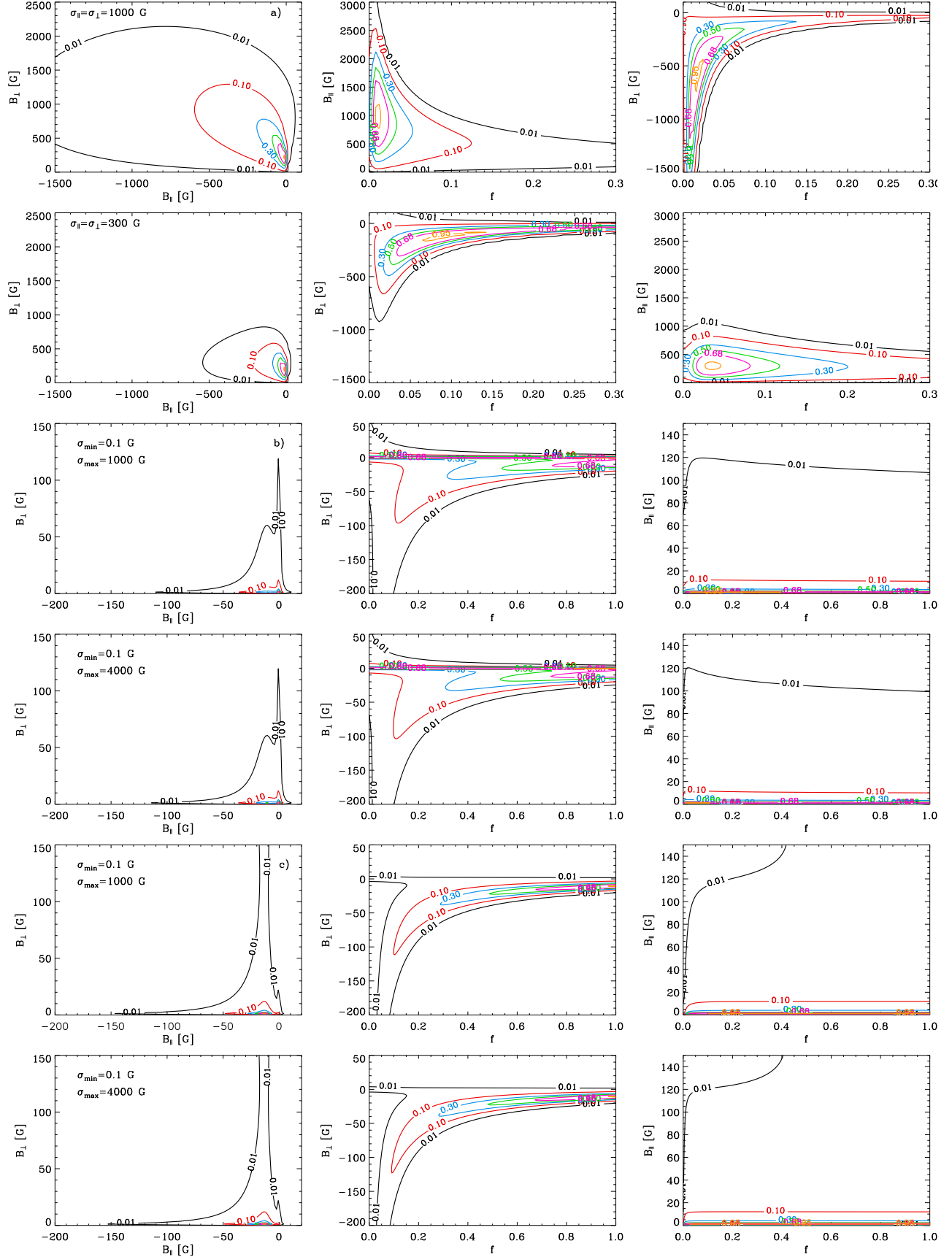


Figure 2. Joint marginal posterior distributions for f , B_{\parallel} and B_{\perp} . The top two rows, labeled with a), correspond to the non-hierarchical case with two different values of σ_{\parallel} and σ_{\perp} . The third and fourth rows, labeled with b), show results with the hierarchical approach of Eq. (33) for two values of σ_{\max} while the last two rows, labeled with c), correspond to the results of the hierarchical model of Eq. (36) for fixed values of $\sigma_{n_{\min}} = 10^{-4}$ and $\sigma_{n_{\max}} = 10^{-2}$ and the two same values for σ_{\min} and σ_{\max} considered in the previous case. For clarity, the contours at normalized probability 0.01, 0.1, 0.3, 0.5, 0.68, 0.95 are marked in black, red, blue, green, magenta and orange, respectively.

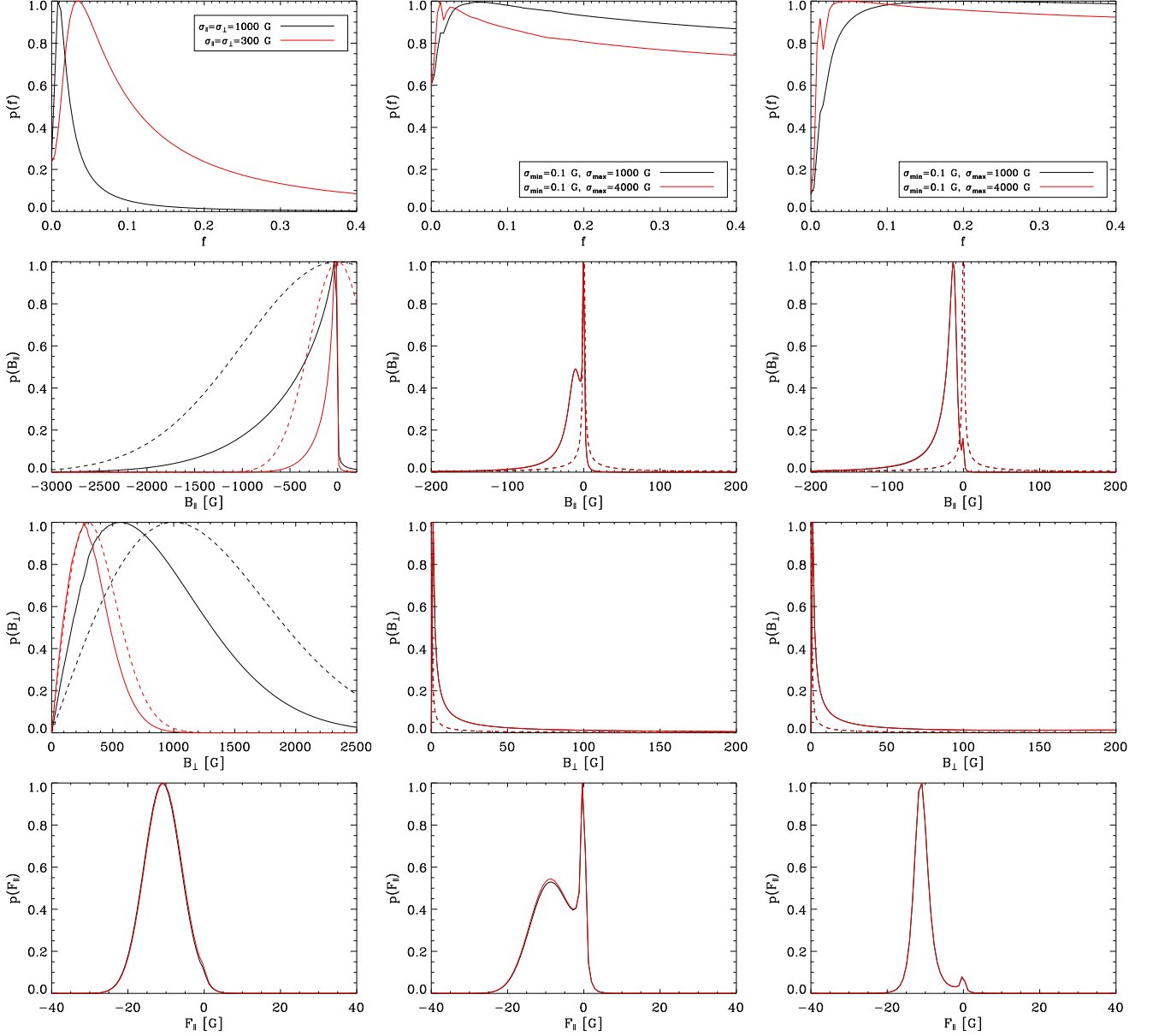


Figure 3. One-dimensional marginal posteriors for f (first row), B_{\parallel} (second row), B_{\perp} (third row) and F_{\parallel} (fourth row). The left column shows the non-hierarchical case, while the second and third columns present results in the two considered hierarchical models. The colors are associated with different values of the hyperparameters. Note the robustness of the hierarchical models to the different values of the hyperparameters. The dashed lines indicate the corresponding prior distribution. If the posterior of a given parameter is clearly different from the prior, we can state that the data contain enough constraining information for this parameter.

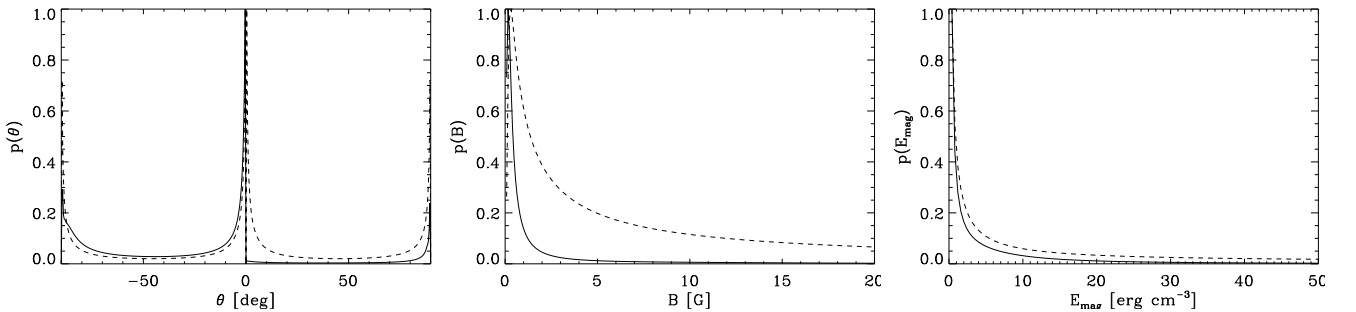


Figure 4. Posterior for derived quantities for the profiles of Fig. 1 using the hierarchical model with $\sigma_n = 2 \times 10^{-3}$, $\sigma_{\min} = 0.1$ G and $\sigma_{\max} = 4000$ G. The left panel shows the marginal posterior for the field inclination, θ , in solid line, while the prior is shown in dashed line. The middle panel presents the marginal posterior for the field strength, while the right panel shows the same for the magnetic energy.

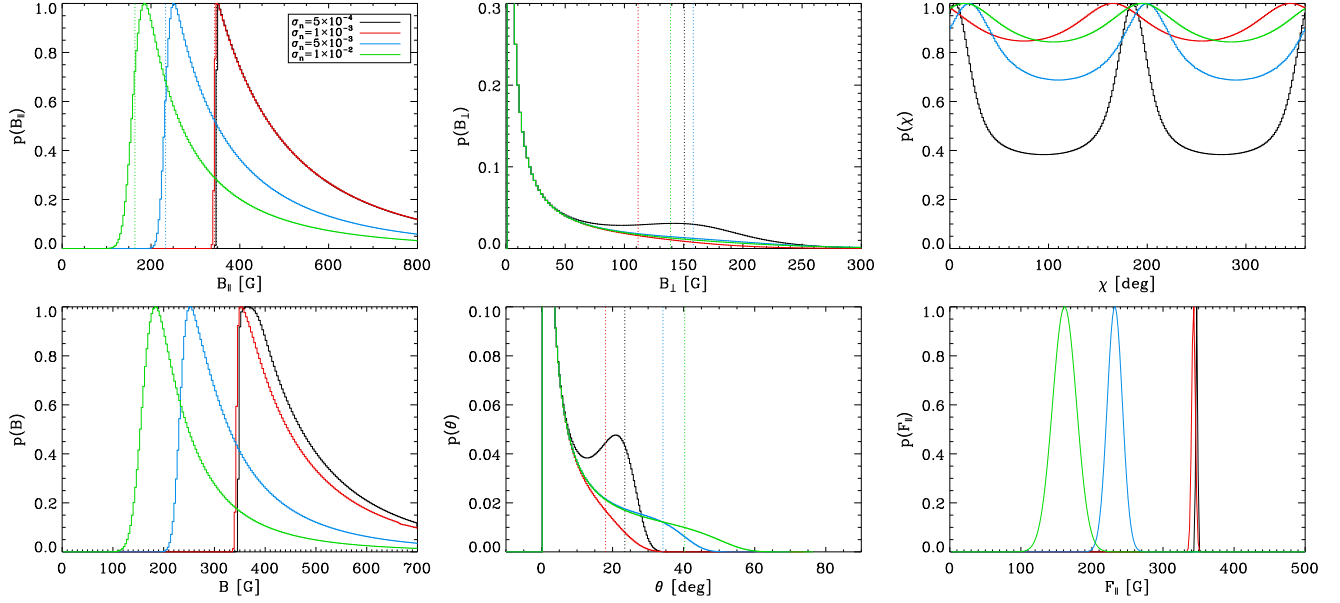


Figure 5. Marginal posteriors for all physical parameters of relevance of a synthetic Stokes profiles with increasingly higher noise levels. The different colors correspond to different noise levels. The vertical dotted lines indicate the maximum-likelihood solution.

Gregory, P. C. 2005, *Bayesian Logical Data Analysis for the Physical Sciences* (Cambridge: Cambridge University Press)

Jeffreys, H. 1961, *Theory of Probability* (Oxford: Oxford University Press)

Jordan, S., Werner, K., & O'Toole, S. J. 2005, *A&A*, 432, 273

Keller, C. U., Steiner, O., Stenflo, J. O., & Solanki, S. K. 1990, *A&A*, 233, 583

Lagg, A., Woch, J., Krupp, N., & Solanki, S. K. 2004, *A&A*, 414, 1109

Landi Degl'Innocenti, E., & Landi Degl'Innocenti, M. 1973, *Sol. Phys.*, 31, 319

—. 1977, *A&A*, 56, 111

Landi Degl'Innocenti, E., & Landolfi, M. 2004, *Polarization in Spectral Lines* (Kluwer Academic Publishers)

Lites, B. W., & Skumanich, A. 1990, *ApJ*, 348, 747

MacKay, D. J. C. 2003, *Information Theory, Inference, and Learning Algorithms* (Cambridge University Press)

Martínez González, M. J., Asensio Ramos, A., López Ariste, A., & Manso Sainz, R. 2008, *A&A*, 479, 229

Martínez González, M. J., & Bellot Rubio, L. R. 2009, *ApJ*, 700, 1391

Martínez Pillet, V., Bonet, J. A., Collados, M. V., Jochum, L., Mathew, S., Medina Trujillo, J. L., Ruiz Cobo, B., del Toro Iniesta, J. C., Lopez Jimenez, A. C., Castillo Lorenzo, J., Herranz, M., Jeronimo, J. M., Mellado, P., Morales, R., Rodriguez, J., Alvarez-Herrero, A., Belenguer, T., Heredero, R. L., Menendez, M., Ramos, G., Reina, M., Pastor, C., Sanchez, A., Villanueva, J., Domingo, V., Gasent, J. L., & Rodriguez, P. 2004, in *Society of Photo-Optical Instrumentation Engineers (SPIE) Conference Series*, Vol. 5487, Society of Photo-Optical Instrumentation Engineers (SPIE) Conference Series, ed. J. C. Mather, 1152–1164

Martínez Pillet, V., Del Toro Iniesta, J. C., Álvarez-Herrero, A., Domingo, V., Bonet, J. A., González Fernández, L., López Jiménez, A., Pastor, C., Gasent Blesa, J. L., Mellado, P., Piqueras, J., Aparicio, B., Balaguer, M., Ballesteros, E., Belenguer, T., Bellot Rubio, L. R., Berkefeld, T., Collados, M., Deutsch, W., Feller, A., Girela, F., Grauf, B., Heredero, R. L., Herranz, M., Jerónimo, J. M., Laguna, H., Meller, R., Menéndez, M., Morales, R., Orozco Suárez, D., Ramos, G., Reina, M., Ramos, J. L., Rodríguez, P., Sánchez, A., Uribe-Patarroyo, N., Barthol, P., Gandorfer, A., Knoelker, M., Schmidt, W., Solanki, S. K., & Vargas Domínguez, S. 2011, *Sol. Phys.*, 268, 57

Merenda, L., Trujillo Bueno, J., Landi Degl'Innocenti, E., & Collados, M. 2006, *ApJ*, 642, 554

Orozco Suárez, D., Bellot Rubio, L. R., del Toro Iniesta, J. C., Tsuneta, S., Lites, B. W., Ichimoto, K., Katsukawa, Y., Nagata, S., Shimizu, T., Shine, R. A., Suematsu, Y., Tarbell, T. D., & Title, A. M. 2007, *ApJ*, 670, L61

O'Toole, S. J., Jordan, S., Friedrich, S., & Heber, U. 2005, *A&A*, 437, 227

Ruiz Cobo, B., & del Toro Iniesta, J. C. 1992, *ApJ*, 398, 375

Silvester, J., Neiner, C., Henrichs, H. F., Wade, G. A., Petit, V., Alecian, E., Huat, A., Martayan, C., Power, J., & Thizy, O. 2009, *MNRAS*, 398, 1505

Skumanich, A., & Lites, B. W. 1987, *ApJ*, 322, 473

Socas-Navarro, H., Trujillo Bueno, J., & Ruiz Cobo, B. 2000, *ApJ*, 530, 977

Solanki, S. K., Barthol, P., Danilovic, S., Feller, A., Gandorfer, A., Hirzberger, J., Riethmüller, T. L., Schüssler, M., Bonet, J. A., Martínez Pillet, V., del Toro Iniesta, J. C., Domingo, V., Palacios, J., Knölker, M., Bello González, N., Berkefeld, T., Franz, M., Schmidt, W., & Title, A. M. 2010, *ApJ*, 723, L127

Spirock, T. J., Denker, C., Varsik, J., Shumko, S., Qiu, J., Gallagher, P., Chae, J., Goode, P., & Wang, H. 2001, *AGU Spring Meeting Abstracts*, 51

Varsik, J. R. 1995, *Sol. Phys.*, 161, 207

Wade, G. A., Donati, J., Landstreet, J. D., & Shorlin, S. L. S. 2000, *MNRAS*, 313, 851